ADVANCED MATERIALS
www.advmat.de

Superaligned Carbon Nanotubes Guide Oriented Cell Growth and Promote Electrophysiological Homogeneity for Synthetic Cardiac Tissues

Jing Ren, Quanfu Xu, Xiaomeng Chen, Wei Li, Kai Guo, Yang Zhao, Qian Wang, Zhitao Zhang, Huisheng Peng, and Yi-Gang Li**

Cardiac engineering of patches and tissues is a promising option to restore infarcted hearts, by seeding cardiac cells onto scaffolds and nurturing their growth in vitro. However, current patches fail to fully imitate the hierarchically aligned structure in the natural myocardium, the fast electrotonic propagation, and the subsequent synchronized contractions. Here, superaligned carbon-nanotube sheets (SA-CNTs) are explored to culture cardiomyocytes, mimicking the aligned structure and electrical-impulse transmission behavior of the natural myocardium. The SA-CNTs not only induce an elongated and aligned cell morphology of cultured cardiomyocytes, but also provide efficient extracellular signal-transmission pathways required for regular and synchronous cell contractions. Furthermore, the SA-CNTs can reduce the beat-to-beat and cell-to-cell dispersion in repolarization of cultured cells, which is essential for a normal beating rhythm, and potentially reduce the occurrence of arrhythmias. Finally, SA-CNT-based flexible one-piece electrodes demonstrate a multipoint pacing function. These combined high properties make SA-CNTs promising in applications in cardiac resynchronization therapy in patients with heart failure and following myocardial infarctions.

Myocardial infarctions are caused by the complete occlusion of coronary arteries, leading to life-threatening losses of downstream myocardium. Lost cardiomyocytes are gradually replaced by heterogeneous fibrous tissue, accompanied with arrhythmogenic inhomogeneous electrophysiological distributions.[1–3] Despite current optimal clinical therapies, postinfarction heart failure, and malignant arrhythmias remain therapeutic challenges.[4] Cardiac engineering of patches and tissues is a promising option to restore infarcted hearts.[5] By seeding cardiac cells onto scaffolds and nurturing their growth in vitro, engineered tissues are expected to generate natural heart structures and functions and can be transplanted to replace fibrous scars.[6,7] Precisely designed scaffolds have been used to organize cells into functional tissues, as in the cases of polymer scaffolds with special structures that guide morphologies of cultured cells[8,9] and the use of conductive components that improve internal cardiac electrical connections.[10,11] In fact, the natural myocardium possesses a hierarchically aligned structure with different layers.[12] For a healthy heart, centripetal synchronous contractions are triggered by electrical impulses propagating along the cardiac conduction system.[13] Thus, elongated and aligned morphologies and electrical signal propagation should be considered during cardiac tissue cultivation.

Carbon nanotubes (CNTs) have been used as additives to improve the mechanical strength and conductivity of bioengineered scaffolds.[14,15] The unique one-dimensional hollow structure, large specific surface area, and good electrical and mechanical properties make CNTs a promising material for sensing,[16] drug releasing,[17] intracellular protein and gene delivering,[18,19] and other tissue engineering applications.[20,21] Previous studies have shown that CNT composite scaffolds can interact with excitable cells, promote cell proliferation and maturation, and induce stem cell differentiation.[22–25] However, randomly dispersed CNTs have been shown to be more likely to form microaggregates and penetrate into cells, leading to inefficient electrical transfer in scaffolds and severe cytotoxicity.[26]

Recently, we applied superaligned CNTs in energy harvesting and storage devices due to its anisotropic structure and remarkable electronic and mechanical properties.[27–29] The advantages of superaligned CNTs can also be transferred in other applications such as promoting biocompatibility, increasing conductivity, and emulating the aligned morphology of the natural myocardium. However, to the best of our knowledge, superaligned CNT materials have not been used for cardiac-related applications. In this Communication, we used superaligned CNT sheets (SA-CNTs) to culture neonatal rat cardiomyocytes

Dr. J. Ren, Dr. Q. Xu, Dr. X. Chen, Dr. W. Li, Dr. K. Guo, Q. Wang, Prof. Y-G. Li
Xinhua Hospital Affiliated to Shanghai Jiao Tong University School of Medicine
Shanghai 200092, China
E-mail: liyigang@xinhuamed.com.cn
Y. Zhao, Dr. Z. Zhang, Prof. H. Peng
State Key Laboratory of Molecular Engineering of Polymers
Department of Macromolecular Science and Laboratory of Advanced Materials
Fudan University
Shanghai 200438, China
E-mail: penghs@fudan.edu.cn

DOI: 10.1002/adma.201702713

(CMs) in vitro, mimicking the aligned structure and electrical-signal-transfer behavior of the natural myocardium (**Figure 1**a).

Prepared by dry-spinning method, SA-CNTs were light-weight and flexible (Figure 1b), and exhibited an aligned microscopic structure (Figure 1c) that gives rise to a better conductivity along the alignment. CMs were seeded onto the SA-CNTs to cultivate into a biomimetic functional patch (Figure 1d). As a result, the CMs aligned on the SA-CNT scaffold and exhibited an elongated cell morphology. Also, an extracellular signal-transmission pathway was established, which could promote regular and synchronous contractions of all cultured CMs. Moreover, beat-to-beat and cell-to-cell dispersions of repolarization were reduced, which is essential for normal beating rhythm. This study demonstrated the preliminary application of SA-CNTs in cardiac pacing, which could be useful to cardiac resynchronization therapy in patients with heart failure following myocardial infarction.

The SA-CNTs were dry-drawn from a spinnable CNT forest synthesized via chemical vapor deposition (CVD) without further chemical modifications (Figure S1a, Supporting Information).[30,31] The CNTs in the forest typically have 6–10 walls and a diameter of ≈10 nm (Figure S1b,c, Supporting Information). The height of the CNT forest varied with growing time. In our case, the height is 200 µm. As shown in scanning electron microscopy (SEM) images, CNTs have a high orientation inside the sheet and there are free space between CNT bundles (Figure S1d, Supporting Information). The Raman spectrum of SA-CNT displays characteristic bands of typical multiwalled CNTs at ≈1340, ≈1580, and ≈2700 cm^{-1} (Figure S2, Supporting Information).[32] Single-layer SA-CNTs are extremely light-weight (≈0.0015 g cm^{-3}).Their thickness is several-hundred nanometers and can be increased by stacking multiple sheets. The width and length of the CNT sheet can be controlled during the dry-spinning process. In our study, three layers of CNT sheets were stacked for cell cultivation (Figure S1e, Supporting Information).

The SA-CNTs have an anisotropic conductivity due to their aligned structure. The conductivity along the alignment is ten times higher than that of the transverse direction (3.1 ± 0.2 mS vs 0.25 ± 0.0 mS, 2.4×2.4 cm^2, $p < 0.01$ (Figure S3, Supporting Information)). SA-CNTs were laid on a nonconductive, flexible and nontoxic poly(dimethylsiloxane) (PDMS) substrate for easier handling. Biodegradable polymers such as calcium alginate gels, collagen, gelatin methacryloyl hydrogels and their composites might be explored for clinical applications in future studies.[33] The CNT-PDMS showed high flexibility. Nearly no resistance change was observed after bending inward for 500 times; a 20% increase was observed after 500 outward bending cycles (the SA-CNTs showed an initial sudden change on the first bend and thereafter stabilized (Figure S4, Supporting Information)). CNTs inside the sheets are bound by Van der Waals force, and they were tightly attached on the PDMS surface by electrostatic attraction. The alignment of CNTs remained after stretching by 30% (Figure S5, Supporting Information). The conductivity of the SA-CNTs can be further increased by stacking more layers of CNT sheets. For example, their conductivity was 4.5 and 77 mS for 5 and 8 layers of SA-CNTs, respectively (Figure S3, Supporting Information).

The biocompatibility of the SA-CNTs was first assessed before their use in CMs culture. Industrial CNT powder is usually synthesized through an arc discharge method using metal catalysts that leaves metallic residues toxic to living cells. The chemical treatment of CNTs was reported to overcome this issue by removing metal catalyst and amorphous carbon.[32] However, our CVD-produced SA-CNTs have very few metal residues, which was confirmed by thermogravimetric analysis (TGA, Figure 1e). A small amount

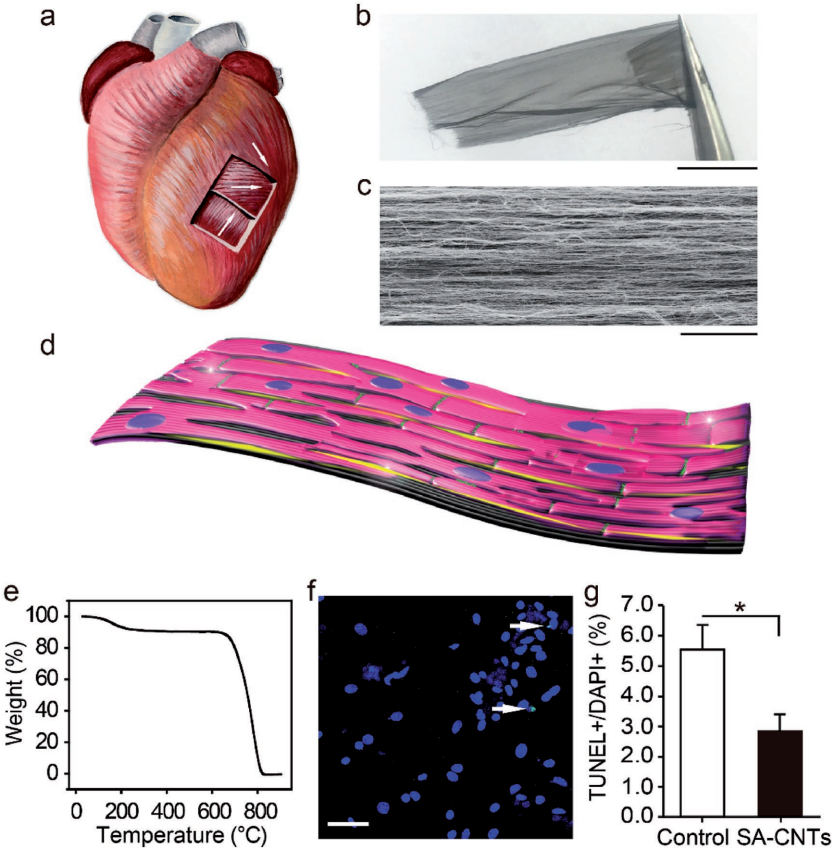

Figure 1. Mimicking the structure of myocardium by SA-CNTs. a) Aligned structure of myocardium in shallow, mid, and deep layers. White arrows indicate the hierarchical orientation of myocardium. b) A flexible three-layer SA-CNTs. Scale bar, 1 cm. c) A representative SEM image of the SA-CNTs. Scale bar, 25 µm. d) Schematic illustration of the conductive SA-CNTs guiding the growth of CMs. e) TGA curve of the SA-CNTs with a heating rate of 10 °C min^{-1} from room temperature to 900 °C. f) The apoptosis assessment of CMs grown on SA-CNTs was labeled using a TUNEL assay (green) for apoptotic cells (arrows) and co-stained with DAPI (blue) for the nucleus. Scale bar: 50 µm. g) Quantitative apoptotic nuclei in total DAPI+ for CMs grown on the coverglass (Control) and SA-CNTs. $n = 5$ for each case from 3 independent experiments. $^*p < 0.05$.

of amorphous carbon first decomposed at 150 °C, followed by the CNTs above 650 °C. When the temperature reached 850 °C, all carbon materials were decomposed and the remaining metal species accounted for less than 0.05% of the total weight.

Apart from having metal residues, randomly dispersed CNTs are prone to form microaggregates. It has been reported that short CNTs can penetrate into living cells, which will interfere with their metabolism and intracellular physiology.[20,26] Nevertheless, the CNTs in the SA-CNTs are hundreds of micrometers in length. They are assembled into aligned bundles that are less likely to enter cells. To study the cytotoxicity of SA-CNTs, randomly-dispersed CNT films (RD-CNTs) were prepared (Experimental Section and Figure S6a, Supporting Information) for comparison and a coverglass for cell culture was used as a control group. CMs were seeded onto SA-CNTs, RD-CNTs or a coverglass and cultured for 4 d. Cytotoxicity was assessed by TUNEL staining of apoptotic cells. Apoptotic nuclei were considered positive when showing a green color, whereas negative live cells only showed blue nuclei.

Confocal microscopy images indicated that the RD-CNTs showed a significantly higher cell death rate of 35.9 ± 2.3% (Figure S6b,d, Supporting Information), whereas the SA-CNTs and the control group had much lower rates of apoptosis (2.9 ± 0.6% and 5.6 ± 0.8%, respectively, $p < 0.05$ (Figure 1f,g and Figure S6c,d, Supporting Information)). The sufficient adhesion of the cells to culture substrates is important for cell extension and growth, and according to our measurements, there was little difference of the CMs' adhesion on the coverglass, RD-CNTs, and SA-CNTs (Experimental Section and Figure S7, Supporting Information). These experiments have shown that SA-CNTs is a safe substrate for culturing cells like CMs.

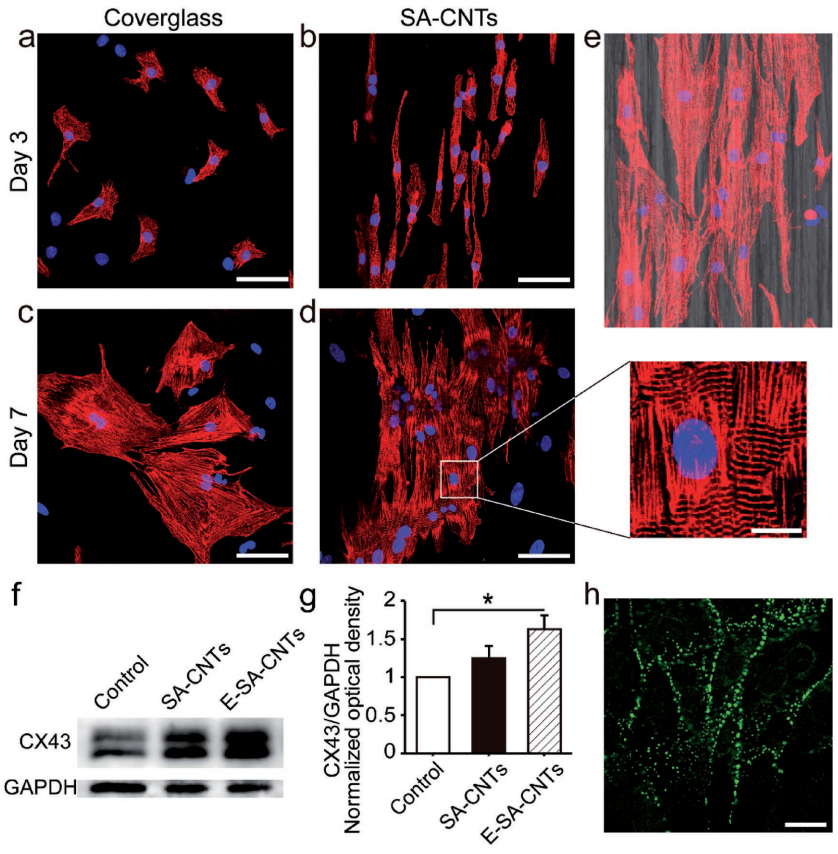

Figure 2. Cell morphology, CX43 expression and distribution. a,b) Representative confocal images indicating that CMs grown on the coverglass (a)extended randomly, while CMs on SA-CNTs (b) elongated along the CNT alignment after 3 d of culture. c,d) Representative images of CMs cultured for 7 d demonstrating that the cells on the coverglass (c) became larger but still kept a random structure, while CMs on SA-CNTs (d) showed oriented distribution with a large amount of massive sarcomeric striations that appeared perpendicular to the oriented direction (d, right panel). e) Representative superimposed confocal image indicating CMs on SA-CNTs along the CNT alignment. f) Representative Western blot showing the expression of CX43 in CMs grown on the coverglass, SA-CNTs and E-SA-CNTs. g) Quantitative Western blot data showing the effects of SA-CNTs and SA-CNTs plus electrical stimulation on Cx43 expression in CMs ($n = 6$ for each case, from three independent experiments). Optical-density signals were normalized to GAPDH and compared with the control (set at 1.0). h) Representative confocal images showing a lateralized linear distribution of CX43 (green) in CMs grown on SA-CNTs after 7 d of culture. *$p < 0.05$. Scale bars: 50 µm (a–e,h), 10 µm (d, right panel).

To achieve elongated cell morphology with the alignment similar to the natural myocardium, we used the SA-CNTs as an aligned scaffold to guide the morphology of CMs. RD-CNTs and coverglasses were used as comparison and control groups, respectively. Morphological evolution of CMs during a 7 d culture period were monitored by confocal microscopy. Confocal images were taken at days 3, 5, and 7, with immunofluorescent staining of α-sarcomeric actinin (red) for the identification of CMs and 4′,6-diamidino-2-phenylindole (DAPI) (blue) for cell nuclei. CMs cultured on coverglasses and RD-CNTs extended in random directions with irregular distributions (**Figure 2**a,c and Figure S8a–f, Supporting Information). In contrast, CMs cultured on SA-CNTs showed an obvious elongated shape parallel to the CNT alignment even at early culturing periods (day 3 (Figure 2b)). At days 5 and 7, CMs on SA-CNTs preserved the elongated shape and aligned morphology and were evenly distributed along the matrix (Figure 2d and Figure S8g–i, Supporting Information). The formation of sarcomeric striations was also observed in CMs on SA-CNTs (Figure 2d, right panel), which reflected the structural maturation of CMs.

These results show that the SA-CNTs can interact with cells and induce the orientation of the growing CMs (Figure 2e and Figure S9, Supporting Information). Because of the isotropic and smooth surface of the coverglasses, the CMs on coverglasses showed evenly extended morphologies (Figure S9a, Supporting Information). However, CMs cultured on RD-CNTs showed an irregular, random morphology at their later culture stages due to the rough surfaces of randomly arranged CNTs (Figure S8f, Supporting Information).

Previous reports have shown that electrical stimulation during CMs culture would increase contractile protein contents

and improve the cell alignment.[34,35] Therefore, after preculture for 48 h, we applied electrical stimulation to CMs by connecting the conductive SA-CNTs to a pacemaker, which continuously outputs a pacing impulse (rectangular, 2 ms, 2 V cm^{-1}, 1 Hz). No measurable heat was generated when the SA-CNTs were subjected to continuous pacing, as shown by thermography (Figure S10, Supporting Information). The apoptosis of CMs grown on electrically stimulated SA-CNTs (E-SA-CNTs) was comparable with those cultured on coverglasses (Figure S11, Supporting Information). A few studies have shown that electrical stimulation also improved the oriented growth of cells.[36,37] However, the morphology of CMs grown on E-SA-CNTs exhibited no notable differences compared with those grown on SA-CNTs without stimulation because the nonstimulated SA-CNTs already showed excellent morphology guidance capabilities (Figure S12, Supporting Information).

CMs are excitable cells capable of receiving and responding to electrical impulses and are responsible for transferring electrical impulses to adjacent cells.[38] Intercellular electrical coupling is accomplished by the gap junction protein connexin-43 (CX43) to ensure the synchronous contraction of all adjoining CMs.[39] Here, we assessed CX43 expression and distribution in different substrates: SA-CNTs, E-SA-CNTs, and RD-CNTs. Coverglasses were used as a control group. Western blotting indicated that CMs cultured on E-SA-CNTs had the highest CX43 level after 5 d of culture (including a 3 d electrical stimulation), suggesting that electrical stimulation enhanced CX43 expression (Figure 2f,g). The SA-CNTs also exerted enhanced CX43 expression, which was independent of the external electrical stimulation (Figure 2f,g and Figure S13, Supporting Information). In contrast, the RD-CNTs had no significant effects on CX43 expression compared with the coverglass or the SA-CNTs (Figure S13, Supporting Information). The labeling of CX43 (green) revealed that the SA-CNTs induced significant lateralized CX43 distribution (with accumulation in intercellular regions), which exhibited alignments consistent with the arrangement of CMs (Figure 2h). Compared with the smooth coverglass and RD-CNTs surfaces, SA-CNTs with electrical stimulation showed multiple effects, including inducing CM orientation during growth and improving intercellular coupling, which would be beneficial to electrical propagation and synchronous contraction.

Aside from affecting the distribution of gap junction proteins, the conductive SA-CNTs were expected to provide a pathway for the rapid conduction of electrical impulses and to ensure the synchronous contraction of all cultured CMs. To assess the contraction behavior of cultured CMs, the contractions of three isolated cell aggregates on each substrate were recorded in situ and analyzed and diagrammed using ImagePro Plus software (Experimental Section, Supporting Information). CMs showed spontaneous contraction on the SA-CNTs and coverglass. However, three isolated cell aggregates on the coverglass contracted with an irregular, asynchronous rhythm, suggesting an arrhythmia (**Figure 3**a,b). In contrast, the three isolated cell aggregates on SA-CNTs showed regular and synchronized contractions even when they were far from each other (Figure 3c,d). This phenomenon indicated that the SA-CNTs created an electrical connection among all cultured CMs, which was beneficial to the synchrony of their beating. It should be noted that the contractility of CMs on SA-CNTs revealed a significant preference along the CNT-aligned direction (contractile ratio of 4.8 ± 0.6%), compared with the traverse direction (contractile ratio of 0.4 ± 0.1%). This phenomenon was not observed in RD-CNTs (Figure S14, Supporting Information). The synchronization of regular contractions well remained within the observation period of 14 d.

To explore the underlying mechanisms of the observed differences in spontaneous beating rhythms, the electrophysiological activities of CMs cultured on different substrates were monitored by whole cell patch clamp techniques at days 3 and 4 (Experimental Section, Supporting Information). The recorded parameters included the resting potential (RP), action potential (AP), action potential amplitude (APA), action potential duration (APD), and AP duration at 30% repolarization (APD_{30}) and 90% repolarization (APD_{90}) (Figure 3e,f and Figure S15 and S16, Supporting Information). Compared with coverglasses, CMs grown on SA-CNTs showed some differences, including more negative resting potentials, higher AP amplitudes, shorter APD_{30} values, and significantly shorter APD_{90} values (Figure 3e,f and Figure S15b,d and S16a,c, Supporting Information), which suggested that SA-CNTs may promote the electrophysiological maturation of neonatal rat CMs,[22] thereby helping cells generate stable and regular beating rhythms.

Additionally, electrophysiological heterogeneities in the infarct-related region have been identified as determinants of postinfarction arrhythmias.[40,41] Available experimental studies have demonstrated that the variability of electrophysiological properties among different cells (cell-to-cell) and among consecutive beats of the same cell (beat-to-beat) are arrhythmogenic factors that favor the occurrence of irregular or chaotic rhythm.[42,43] Thus, the beat-to-beat and cell-to-cell dispersions of APA, RP, APD_{30}, and APD_{90} were analyzed to evaluate electrophysiological heterogeneity. SA-CNTs significantly reduced the high dispersion of APD_{30} (in a cell-to-cell manner) and APD_{90} (in beat-to-beat and cell-to-cell manners) observed in CMs growing on the coverglass (Figure 3g). No other differences were found in the APA or RP dispersions between the SA-CNTs and coverglass (Figure S15c,e, Supporting Information). It should be noted that RD-CNTs also slightly improved the electrophysiological heterogeneity of CMs when compared with that for coverglasses. However, this improvement was smaller than that of the SA-CNTs (Figure S15 and S16, Supporting Information).

We speculate the synchronized regular beating rhythms of CMs growing on SA-CNTs can be explained by the following mechanisms: i) accelerated electrophysiological maturation of neonatal rat CMs and reduced beat-to-beat APD dispersion enabled the cells to generate regular and stable beats; ii) improved intercellular coupling through the increased and lateralized CX43 expression allowed adjacent cells to synchronously contract; iii) reduced cell-to-cell APD dispersions prepared all cells, even those isolated far from each other, to be simultaneously excited upon electrical impulse. Furthermore, SA-CNTs provided an efficient pathway for rapid electronic propagation to all ready-to-excite cells, with stable conductivity and pacing threshold during the observation period of 14 d (Figure S17, Supporting Information). Therefore, SA-CNT-based cardiac tissue patches achieved the synchronized contraction of all

cultured cells with reduced electrophysiological heterogeneity, which provided a potential method to restore the infarcted myocardium and alleviate the electrophysiological heterogeneity in infarct-related regions.

In addition to synchronized spontaneous beating, CMs cultured on SA-CNTs showed synchronous contraction when the SA-CNTs were connected to a pacemaker (**Figure 4**a,b). Three isolated CMs aggregates were monitored at pacing rates from 60 to 100 bpm, indicating fully synchronized contraction and excellent frequency adaptability corresponding to the pacing rate. The SA-CNTs displayed a pacing function through a fast signal-transmitting pathway, which implies further applications in cardiac resynchronization therapy (i.e., an effective therapy in patients with heart failure and ventricular dyssynchrony that sends electrical impulses to the right and left ventricular muscle through two individual leads, thereby synchronously pacing both ventricles for more efficient blood pumping).

SA-CNTs were further developed into a flexible one-piece pacemaker electrode. Cardiac resynchronization therapy has been proved effective, but one third of patients fail to respond.[44] Different areas of a heart (e.g., apex of right ventricle and septum and epicardial wall of the left ventricle) are paced by separate leads. The suboptimal left ventricular lead implantation caused by variations in the coronary venous anatomy is a key factor for the high number of nonresponders under treatment.[45] Accordingly, we developed a one-piece electrode to provide a larger contact area capable of simultaneously covering the right and left ventricles. The porous surface, good conductivity, high flexibility, and light weight make it easy to attach SA-CNTs to soft cardiac tissue to transmit pacing impulses to the myocardium. Here, the synchronous pacing function was tested by arranging three Tyrode's solution-perfused neonatal rat hearts (corresponding to three different parts of a heart(Figure S18, Supporting Information)) onto a pacemaker connected to SA-CNTs in vitro and simultaneously monitoring their ventricular monophasic action potentials (MAPs) (Figure S19, Supporting Information). Continuous MAP tracing demonstrated that the SA-CNTs provided a synchronous pacing of these isolated hearts (rectangular, 2 ms, 2 V cm^{-1}, 1 Hz), showing a nondistinctive beating rhythm (Figure 4c). Indium tin oxide (ITO) glass, a common inorganic material with high isotropic electrical conductivity (sheet resistance <10 Ω cm^{-2}), was also tested as a one-piece electrode for pacing isolated hearts. However, the MAP tracing of two hearts on ITO glass failed to capture ventricles during cardiac pacing even at a maximal pacing voltage of 10 V (Figure 4c).

This phenomenon can be explained by the fact that the internal resistance of the ITO glass electrode was much lower

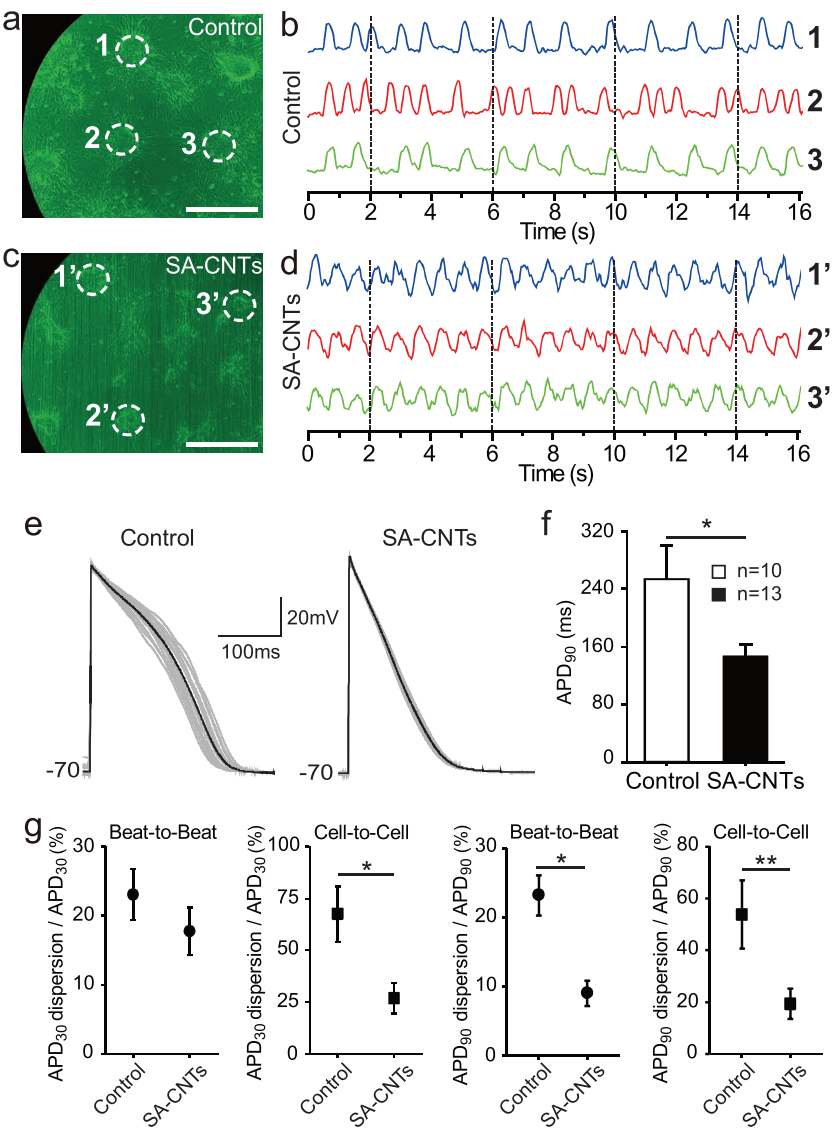

Figure 3. Contractile behavior of cardiomyocytes grown on SA-CNTs and their electrophysiological characteristics. a,c) Phase contrast images demonstrating isolated CM aggregates grown on the coverglass (a) and SA-CNTs (c) after culture for 4 d. A brightness change was detected for contractile behavior tracing. Scale bar, 500 µm. b,d) Traces of spontaneous contractions of three isolated CM aggregates cultured on the coverglass showing irregular and asynchronous contractions (b) while those on SA-CNTs showing regular, stable, and synchronous contractions (d). e) Representative evoked APs of CMs cultured on the coverglass (Control) and SA-CNTs after 3–4 d of culture. Gray traces are recordings of evoked APs, while the superimposed black traces represent the average of 18 trials. f) Comparison of APD_{90} between CMs grown on the coverglass (Control) and SA-CNTs. $*p < 0.05$. g) Comparison of APD_{30} and APD_{90} dispersions between CMs grown on the coverglass (Control) and SA-CNTs in the manner of beat-to-beat and cell-to-cell. $*p < 0.05$, $**p < 0.01$. APD dispersion = $APD_{Max} - APD_{Min}$, and APD dispersion was adjusted with APD. $n = 7$ for control sample and $n = 9$ for SA-CNTs from 3 independent experiments (beat-to-beat dispersion), and $n = 5$ for control sample and $n = 7$ for SA-CNTs from 3 independent experiments (cell-to-cell dispersion).

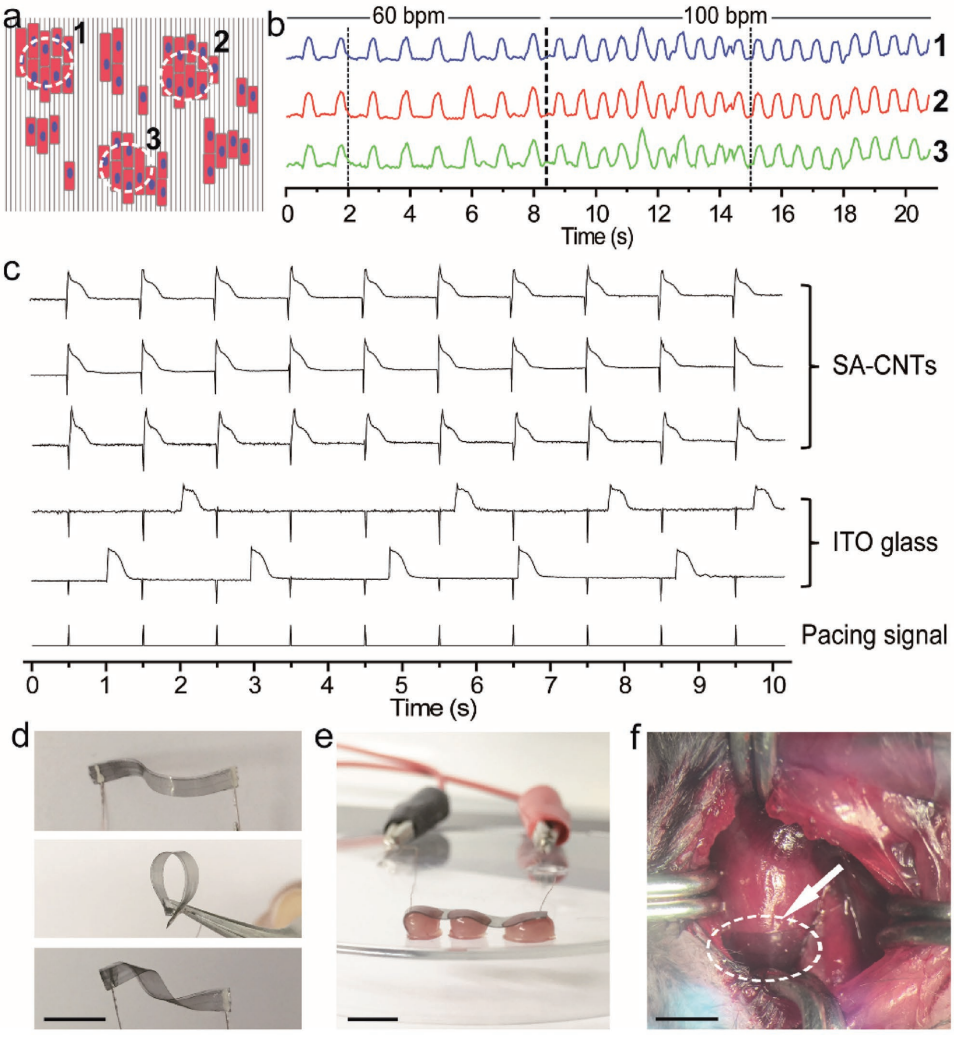

Figure 4. One-piece pacemaker electrode enabled for cardiac pacing and resynchronization therapy. a) Schematic of three isolated CM aggregates grown on SA-CNTs after a 4 d culture to detect their brightness change for contractile behavior tracing. b) Representative traces indicating synchronous pacing of three isolated CM aggregates through SA-CNTs by a pacemaker at a rate of 60–100 bpm. c) MAP tracing of three Tyrode's solution perfused neonatal rat hearts on SA-CNTs (upper panel) showing synchronized beating under pacing at 1 Hz (rectangular, 2 ms, 2 V cm^{-1}), and MAP tracing of two hearts on the conductive ITO glass (lower panel) demonstrating the failure of ventricular capture during cardiac pacing even at the maximal pacing voltage of 10 V. These two individual hearts only displayed spontaneous asynchronous contractions. d) SA-CNTs laid on PDMS showing a high flexibility. e) SA-CNTs attached properly to three isolated neonatal rat hearts, imitating the application in cardiac resynchronization therapy in patients with heart failure. f) SA-CNTs showing good attachment to the surface of a live mouse heart under cardiac pacing. Scale bars, 0.3 cm d,f). Scale bar, 0.5 cm e).

than the contact resistance between the electrode and the tissue, which caused a short circuit. Therefore, the electric pulse was unable to be properly transmitted to the tissue. However, the SA-CNTs performed an excellent synchronous pacing function at the cellular and tissue levels possibly due to appropriate conductivity and good surface adhesion. The study of the relationship between the internal resistance of the electrode material and the contact resistance is underway. A thin, flexible one-piece pacing SA-CNT electrode was fabricated to synchronously pace three isolated hearts, imitating the application in cardiac resynchronization therapy (Figure 4d,e and Figure S19 and Video S1, Supporting Information). This flexible one-piece electrode could also pace a mouse heart in vivo and showed an excellent attachment and pacing function (Figure 4f and Video S2, Supporting Information).

In summary, we show that SA-CNTs can efficiently guide the cell morphology and provide electrical transmission pathways for cardiac tissue engineering. CMs cultured on SA-CNTs have improved intercellular coupling, reduced repolarization dispersion, and synchronized spontaneous beatings. Electrically stimulated SA-CNTs synergistically promote the maturation of neonatal rat CMs. Flexible one-piece SA-CNT electrodes show excellent tissue attachment and pacing function. Thus, SA-CNTs can be potentially applied for inducing the recovery of infarcted hearts with injured structural and electrical functions.

Supporting Information

Supporting Information is available from the Wiley Online Library or from the author.

Acknowledgements

J.R. and Q.X. contributed equally to this work. This work was supported by the Shanghai Sailing Program (17YF1411500 and 14YF1402900), the China Postdoctoral Science Foundation Grant (2017M610263), the State Key Program of National Natural Science Foundation of China (No. 81530015), MOST (No. 2016YFA0203302), NSFC (Nos. 81270258, 21634003, 51573027, 51403038, and 51673043), and STCSM (Nos. 14441902502, 16JC1400702, 15XD1500400, and 15JC1490200). The authors declare no conflict of interests in this work. The authors would like to thank Qing Zhou, Rui Zhang, and Yihe Chen for excellent technical assistance. Special thanks to Xin Fang at University of Cambridge for language revision, useful discussion, and great support. All animal experiments were approved by the Institutional Animal Care and Use Committee of Xinhua Hospital in accordance with the Guide for the Care and Use of Laboratory Animal published by the National Institutes of Health (Approval No, XHEC-F-2016-038).

Conflict of Interest

The authors declare no conflict of interest.

Keywords

aligned materials, carbon nanotubes, cardiac pacing, cardiac tissue, sheets

Received: May 15, 2017
Revised: July 19, 2017
Published online: October 11, 2017

[1] P. Gaudron, C. Eilles, I. Kugler, G. Ertl, *Circulation* **1993**, *87*, 755.
[2] M. G. Kienzle, J. U. Doherty, D. Cassidy, A. E. Buxton, F. E. Marchlinski, H. L. Waxman, M. E. Josephson, *Am. J. Cardiol.* **1986**, *58*, 63.
[3] M. Mollenhauer, K. Friedrichs, M. Lange, J. Gesenberg, L. Remane, C. Kerkenpass, J. Krause, J. Schneider, T. Ravekes, M. Maass, M. Halbach, G. Peinkofer, T. Saric, D. Mehrkens, M. Adam, F. G. Deuschl, D. Lau, B. Geertz, K. Manchanda, T. Eschenhagen, L. Kubala, T. K. Rudolph, Y. Wu, W. W. Tang, S. L. Hazen, S. Baldus, A. Klinke, V. Rudolph, *Circ. Res.* **2017**, *121*, 56.
[4] G. Pizarro, L. Fernandez-Friera, V. Fuster, R. Fernandez-Jimenez, J. M. Garcia-Ruiz, A. Garcia-Alvarez, A. Mateos, M. V. Barreiro, N. Escalera, M. D. Rodriguez, A. de Miguel, I. Garcia-Lunar, J. J. Parra-Fuertes, J. Sanchez-Gonzalez, L. Pardillos, B. Nieto, A. Jimenez, R. Abejon, T. Bastante, V. Martinez de Vega, J. A. Cabrera, B. Lopez-Melgar, G. Guzman, J. Garcia-Prieto, J. G. Mirelis, J. L. Zamorano, A. Albarran, J. Goicolea, J. Escaned, S. Pocock, A. Iniguez, A. Fernandez-Ortiz, V. Sanchez-Brunete, C. Macaya, B. Ibanez, *J. Am. Coll. Cardiol.* **2014**, *63*, 2356.
[5] B. Tian, J. Liu, T. Dvir, L. Jin, J. H. Tsui, Q. Qing, Z. Suo, R. Langer, D. S. Kohane, C. M. Lieber, *Nat. Mater.* **2012**, *11*, 986.
[6] B. Zhang, M. Montgomery, M. D. Chamberlain, S. Ogawa, A. Korolj, A. Pahnke, L. A. Wells, S. Masse, J. Kim, L. Reis, A. Momen, S. S. Nunes, A. R. Wheeler, K. Nanthakumar, G. Keller, M. V. Sefton, M. Radisic, *Nat. Mater.* **2016**, *15*, 669.
[7] L. Gao, M. E. Kupfer, J. P. Jung, L. Yang, P. Zhang, Y. Da Sie, Q. Tran, V. Ajeti, B. T. Freeman, V. G. Fast, P. J. Campagnola, B. M. Ogle, J. Zhang, *Circ. Res.* **2017**, *120*, 1318.
[8] G. C. Engelmayr Jr., M. Cheng, C. J. Bettinger, J. T. Borenstein, R. Langer, L. E. Freed, *Nat. Mater.* **2008**, *7*, 1003.
[9] M. E. Kolewe, H. Park, C. Gray, X. Ye, R. Langer, L. E. Freed, *Adv. Mater.* **2013**, *25*, 4459.
[10] T. Dvir, B. P. Timko, M. D. Brigham, S. R. Naik, S. S. Karajanagi, O. Levy, H. Jin, K. K. Parker, R. Langer, D. S. Kohane, *Nat. Nanotechnol.* **2011**, *6*, 720.
[11] B. Yang, F. Yao, T. Hao, W. Fang, L. Ye, Y. Zhang, Y. Wang, J. Li, C. Wang, *Adv. Healthcare Mater.* **2016**, *5*, 474.
[12] J. B. Caulfield, T. K. Borg, *Lab Invest.* **1979**, *40*, 364.
[13] L. Padeletti, R. Lieberman, S. Valsecchi, D. A. Hettrick, *Pacing Clin. Electrophysiol.* **2006**, *29* (Suppl 2), S73.
[14] S. Pok, F. Vitale, S. L. Eichmann, O. M. Benavides, M. Pasquali, J. G. Jacot, *ACS Nano* **2014**, *8*, 9822.
[15] S. R. Shin, R. Farzad, A. Tamayol, V. Manoharan, P. Mostafalu, Y. S. Zhang, M. Akbari, S. M. Jung, D. Kim, M. Comotto, N. Annabi, F. E. Al-Hazmi, M. R. Dokmeci, A. Khademhosseini, *Adv. Mater.* **2016**, *28*, 3280.
[16] F. Seichepine, J. Rothe, A. Dudina, A. Hierlemann, U. Frey, *Adv. Mater.* **2017**, *29*, 1606852.
[17] M. Martincic, G. Tobias, *Expert. Opin. Drug Delivery* **2015**, *12*, 563.
[18] S. R. Ji, C. Liu, B. Zhang, F. Yang, J. Xu, J. Long, C. Jin, D. L. Fu, Q. X. Ni, X. J. Yu, *Biochim. Biophys. Acta* **2010**, *1806*, 29.
[19] A. Masotti, M. R. Miller, A. Celluzzi, L. Rose, F. Micciulla, P. W. Hadoke, S. Bellucci, A. Caporali, *Nanomedicine* **2016**, *12*, 1511.
[20] G. Cellot, E. Cilia, S. Cipollone, V. Rancic, A. Sucapane, S. Giordani, L. Gambazzi, H. Markram, M. Grandolfo, D. Scaini, F. Gelain, L. Casalis, M. Prato, M. Giugliano, L. Ballerini, *Nat. Nanotechnol.* **2009**, *4*, 126.
[21] E. L. Hopley, S. Salmasi, D. M. Kalaskar, A. M. Seifalian, *Biotechnol. Adv.* **2014**, *32*, 1000.
[22] V. Martinelli, G. Cellot, F. M. Toma, C. S. Long, J. H. Caldwell, L. Zentilin, M. Giacca, A. Turco, M. Prato, L. Ballerini, L. Mestroni, *Nano Lett.* **2012**, *12*, 1831.
[23] V. Martinelli, G. Cellot, F. M. Toma, C. S. Long, J. H. Caldwell, L. Zentilin, M. Giacca, A. Turco, M. Prato, L. Ballerini, L. Mestroni, *ACS Nano* **2013**, *7*, 5746.
[24] J. Landers, J. T. Turner, G. Heden, A. L. Carlson, N. K. Bennett, P. V. Moghe, A. V. Neimark, *Adv. Healthcare Mater.* **2014**, *3*, 1745.
[25] M. V. Pryzhkova, I. Aria, Q. Cheng, G. M. Harris, X. Zan, M. Gharib, E. Jabbarzadeh, *Biomaterials* **2014**, *35*, 5098.
[26] A. Bianco, K. Kostarelos, M. Prato, *Chem. Commun.* **2011**, *47*, 10182.
[27] J. Ren, Y. Zhang, W. Bai, X. Chen, Z. Zhang, X. Fang, W. Weng, Y. Wang, H. Peng, *Angew Chem., Int. Ed. Engl.* **2014**, *53*, 7864.
[28] Z. Zhang, Y. Zhang, Y. Li, H. Peng, *Acta Polym. Sin.* **2016**, *10*, 1284.
[29] Z. Yang, J. Ren, Z. Zhang, X. Chen, G. Guan, L. Qiu, Y. Zhang, H. Peng, *Chem. Rev.* **2015**, *115*, 5159.
[30] K. Jiang, Q. Li, S. Fan, *Nature* **2002**, *419*, 801.
[31] M. Zhang, K. R. Atkinson, R. H. Baughman, *Science* **2004**, *306*, 1358.
[32] S. Madani, A. Tan, M. Dwek, A. Seifalian, *Int. J. Nanomed.* **2012**, *7*, 905.
[33] S. Ahadian, S. Yamada, J. R. Azcón, M. Estili, X. Liang, K. Nakajima, H. Shiku, A. Khademhosseini, T. Matsue, *Acta Biomater.* **2016**, *31*, 134.
[34] M. Radisic, H. Park, H. Shing, T. Consi, F. J. Schoen, R. Langer, L. E. Freed, G. Vunjak-Novakovic, *Proc. Natl. Acad. Sci. USA* **2004**, *101*, 18129.
[35] J. L. Ruan, N. L. Tulloch, M. V. Razumova, M. Saiget, V. Muskheli, L. Pabon, H. Reinecke, M. Regnier, C. E. Murry, *Circulation* **2016**, *134*, 1557.

[36] M. Zhao, H. Bai, E. Wang, J. V. Forrester, C. D. McCaig, *J. Cell. Sci.* **2004**, *117*, 397.
[37] H. T. Au, I. Cheng, M. F. Chowdhury, M. Radisic, *Biomaterials* **2007**, *28*, 4277.
[38] G. E. Morley, D. Vaidya, *Microsc. Res. Tech.* **2001**, *52*, 241.
[39] S. A. Thomas, R. B. Schuessler, C. I. Berul, M. A. Beardslee, E. C. Beyer, M. E. Mendelsohn, J. E. Saffitz, *Circulation* **1998**, *97*, 686.
[40] R. Wolk, S. M. Cobbe, M. N. Hicks, K. A. Kane, *Pharmacol. Ther.* **1999**, *84*, 207.
[41] M. J. Bishop, A. Connolly, G. Plank, *PLoS One* **2014**, *9*, e109754.
[42] C. C. Chou, S. Zhou, H. Hayashi, M. Nihei, Y. B. Liu, M. S. Wen, S. J. Yeh, M. C. Fishbein, J. N. Weiss, S. F. Lin, D. Wu, P. S. Chen, *J. Physiol.* **2007**, *580*, 895.
[43] E. Pueyo, C. E. Dangerfield, O. J. Britton, L. Virag, K. Kistamas, N. Szentandrassy, N. Jost, A. Varro, P. P. Nanasi, K. Burrage, B. Rodriguez, *PLoS One* **2016**, *11*, e0151461.
[44] C. Daubert, N. Behar, R. Martins, P. Mabo, C. Leclercq, *Eur. Heart J.* **2017**, *38*, 1463.
[45] A. Roka, R. Borgquist, J. Singh, *Heart Failure Clin.* **2017**, *13*, 79.

